Micro-Tapered-Tubes Flow Analysis via DSMC and Experimental Methods

Christos Tantos, Foteini Litovoli, Franz Schweizer, Lucien Baldas, Juergen J. Brandner, Jan Gerrit Korvink, Thomas Giegerich, and Marcos Rojas-Cárdenas

Abstract A numerical and experimental analysis was performed on pressure-driven flows through micro-tapered tubes, which were fabricated using Two-Photon Polymerization additive manufacturing. Special emphasis was placed on the crucial role of uncertainties associated with the geometric size characterization. The constant volume technique was employed for experimental characterization, and nitrogen was used as the working gas. The DSMC method was utilized for the numerical part. The mass flow rate results show a good agreement between experiments and DSMC, within the numerical and experimental uncertainties. This study highlights the importance of DSMC as an effective tool for flow characterization in 3D microscale structures and of the TPP as a novel manufacturing technique for complex microfluidic devices working with rarefied gas flows.

Keywords Microfluidics · Tapered microchannels · DSMC · Two-photon-polymerization manufacturing

1 Introduction

The correct characterization and modeling of gas flows in microdevices enables the further development of micro-electro-mechanical systems (MEMS). As an extension of constant cross-section tubes and channels, tapered flow configurations are of

C. Tantos (✉) · F. Litovoli · T. Giegerich
Institute for Technical Physics (ITEP), Karlsruhe Institute of Technology (KIT), Karlsruhe, Germany
e-mail: christos.tantos@kit.edu

F. Schweizer · J. J. Brandner · J. G. Korvink
Institute of Microstructure Technology (IMT), Karlsruhe Institute of Technology (KIT), Karlsruhe, Germany

F. Schweizer · L. Baldas · M. Rojas-Cárdenas
Institut Clément Ader (ICA), Université de Toulouse, CNRS, INSA Toulouse, ISAE-SUPAERO, IMT Mines Albi, UT3, Toulouse, France

M. Grabe et al. (eds.), *Rarefied Gas Dynamics*, Springer Aerospace Technology,
https://doi.org/10.1007/978-3-032-00094-1_23

increasing interest, because of their potential applications in various technological fields, including aerospace [1] and vacuum technologies [2].

Over the past decade, gas flow through tapered channels has become an increasingly attractive area of study for modelers in the rarefied gas dynamics community. These types of flow configurations have been studied throughout a wide range of gas rarefaction using mainly two different numerical approaches. The first approach, originally proposed in [3] for long tubes of variable radius, is based on mass conservation and its main advantage is that, as a 1D method, it allows fast calculations of the mass flow rate and pressure distribution along the flow direction. Due to its simplicity, this methodology has also been applied to analyze single gas flows through rectangular channels with variable cross-section [4]. Its effectiveness is well-established for channels with large length-to-radius ratios and relatively low variations of radius along the axis of the channel [5, 6]. The second approach is more computationally demanding and involves the complete solution of the flow field within the tapered channel using either Direct Simulation Monte Carlo (DSMC) or Discrete Velocity Method (DVM). Several studies in the literature have used the DSMC or DVM methods to investigate flows through diverging or converging channels, formed by parallel plates placed at a relative angle to each other [6–8]. To the best of our knowledge, most experimental studies on tapered micro-channels focus on planar geometries [1], with limited modeling of tapered tubes [5].

The scope of the present work is to study the computed and measured mass flow rates in pressure-driven flows through micro-tapered tubes manufactured via Two-photon-polymerization additive fabrication technique. Specific attention was given to the analysis of the crucial role of geometric size characterization. The paper is organized as follows. In Sect. 2, the experimental setup and the fabrication of the tapered channel are described. In Sect. 3, the simulated flow configuration and the numerical results are analyzed. In Sect. 4, the experimental and numerical results are presented and discussed, and in Sect. 5 the main conclusions are summarized.

2 Experimental Setup Methodology (Fabrication and the Characterization of the Tapered Channel)

The tapered channel structure was fabricated using Two-Photon-Polymerization (TPP), which is an additive manufacturing technique based on the local polymerization of a liquid photosensitive resin. This fabrication technique was previously utilized for the fabrication of straight microtubes for rarefied gas flows applications [9]. The working principle of the manufacturing technique is illustrated in Fig. 1a. After a droplet of resin (IP-Q, Nanoscribe GmbH) is deposited on a substrate, a femtosecond pulsed laser is focused and directed through the resin with controlled trajectory. The resin solidifies when the threshold of energy intensity is reached. This is only the case in the focus point of the laser, thus generating ellipsoidal voxels. The structure was fabricated by overlapping these ellipsoidal voxels with a slicing distance of 5

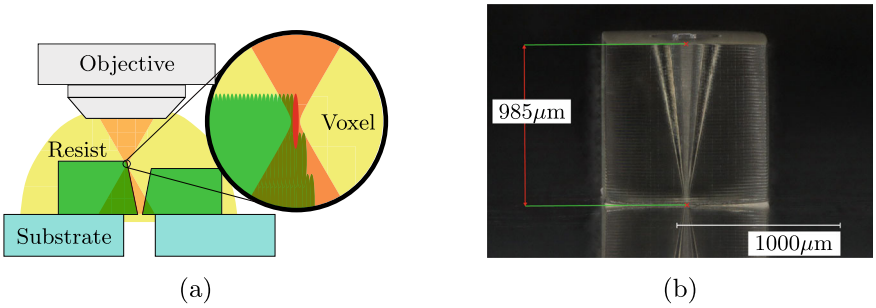

Fig. 1 **a** Schematic of the TPP process; **b** microscope image of the tapered channel

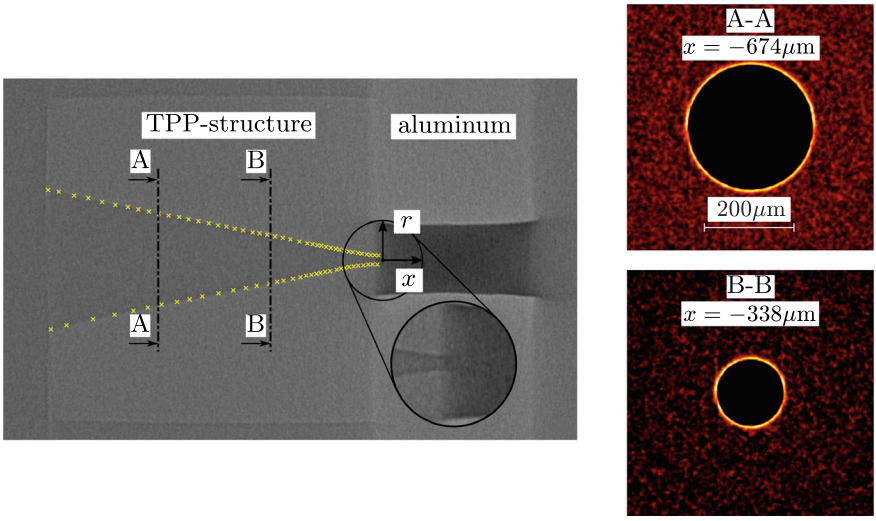

Fig. 2 Tomography image with radius measurement points and cross-sections. Not all measurement points are shown to avoid the overlapping of measurement markers

µm and a lateral hatching distance of 1 µm. After the printing process the sample was submerged in propylene glycol methylether acetate (PGMEA) for a total of 14 h to dissolve the uncured resin. Lastly the structure was rinsed in a solvent and left to dry at 7 °C for 30 min. The fabrication process therefore took approximately 15.5 h, including a printing time of 1 h.

As visible in Fig. 1b the tapered channel was written inside a polymer cube of roughly 1 mm × 1 mm × 1 mm. The structure was deposited on an aluminum substrate of the dimensions 25 mm × 25 mm × 0.5 mm. Furthermore the aluminum substrate encompasses a circular orifice of 200 µm in diameter. This orifice is aligned with the channel to enable the connection of the nozzle of the channel to the experimental setup (Fig. 2). The radius of the channel varies linearly from 215–14 µm over a length of 1012 µm. A high aspect ratio microtube with a circular cross-section,

Table 1 **a** Coefficient values of the polynomials for the radius function $R(x)$; **b** experimental campaign initial conditions

(a)

a_0	13.6 μm
a_1	0.01597
a_2	2.57822e-3 μm^{-1}
a_3	1.868179e-5 μm^{-2}
a_4	9.156089e-8 μm^{-3}
a_5	3.0165235e-10 μm^{-4}
a_6	6.5164167e-13 μm^{-5}
a_7	8.9978361e-16 μm^{-6}
a_8	7.6065986e-19 μm^{-7}
a_9	3.5761114e-22 μm^{-8}
a_{10}	7.150218e-26 μm^{-9}
b_0	111.1 μm
b_1	-6.83e-2
b_2	2.09e-4 μm^{-1}
b_3	-7.9e-08 μm^{-2}

(b)

	Converging		Diverging	
Case	P_A [Pa]	P_B [Pa]	P_A [Pa]	P_B [Pa]
1	210.0	10.0	10.0	206.4
2	303.3	103.2	104.3	304.3
3	409.0	209.0	205.1	401.4
4	505.0	209.0	305.3	505.3
5	604.0	404.0	405.5	599.6
6	705.1	505.1	504.8	700.4
7	800.2	600.2	602.4	802.4
8	902.2	702.2	703.6	901.0
9	1001.7	802.1	802.9	999.7
10	1104.2	904.2	902.6	1097.1
11	1202.4	1002.4	1001.6	1197.8
12	1298.9	1099.1	1101.0	1297.1

whose size varies, is thus obtained. Previous experimental investigations of tapered microchannels have mostly relied on standard planar micro-machining of silicon [1] or micro-milling of metals [10]. Owing to the limitations of these methods only rectangular cross-sections were investigated.

The geometry of the present channel was characterized using a EasyTom XL tomograph (RX Solutions). The resulting tomograms showed an isotropic pixel size of 2.77 μm and were analyzed to extract the internal geometry of the channel. The diameter variation along the length of the channel was measured on the symmetry plane of the channel (Fig. 2, left). The geometry measurement was performed via an edge detection algorithm. Since the nozzle geometry has a critical influence on the flow field, a higher number of measurements were obtained for this region. Furthermore, as it can be seen in Fig. 2 (right), the circularity of the tapered channel cross-section is of excellent quality. To smooth the measurement results, two polynomials were used: the $10th$ order polynomial for the tapered channel section ($R(x) = \sum_{i=0}^{10} a_i x^i$, $-1012\ \mu m \leq x \leq 0$) and a $3rd$ order polynomial for the section inside of the aluminum substrate ($R(x) = \sum_{j=0}^{3} b_j x^j$, $0 \leq x \leq 458\ \mu m$). The coefficients of the polynomials are given in Table 1a.

The flow properties of the channel structure were experimentally investigated utilizing the constant volume technique. This very well established technique relates pressure variation to mass variation in a constant volume [9, 11, 12]. The experimental methodology consisted in setting an initial pressure difference between inlet and outlet of the tapered channel and then allowing the thermodynamic system to relax to equilibrium. The mass flow rate generated through the channel creates a pressure

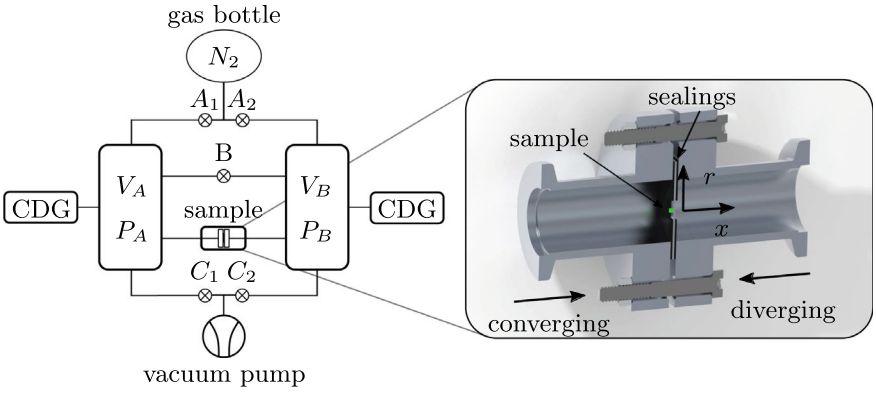

Fig. 3 Constant volume technique experimental setup and sample clamping technique

variation in the inlet and outlet tanks. The initial pressure conditions are specificied in Table 1b. Figure 3 shows a schematic of the used flow setup. The substrate of the flow sample was clamped in a casing using rubber seals. Furthermore the sample was connected to the two volumes V_A and V_B where the pressures P_A and P_B were acquired by Capacitance Diaphragm Gauges (CDG) with full ranges of 1333 Pa and an accuracy of 0.2% of reading. The average pressure and applied pressure difference in the setup could be controlled through the valves $A_{1,2}$ and $C_{1,2}$ which were connected to a pressurized nitrogen bottle and a vacuum pump. This setup allowed initial conditions $P_A > P_B$ for converging flow experiments and $P_A < P_B$ for diverging flow experiments.

The mass flow rate from the volumes and therefore through the sample can be calculated using the ideal gas law assuming isothermal conditions in the volumes $V_{A,B}$ as

$$\dot{m}_{A,B} = \frac{V_{A,B}}{R_g T_0} \frac{\mathrm{d}P_{A,B}}{\mathrm{d}t}, \tag{1}$$

with R_g and T_0 being the specific gas constant and the temperature in the experimental room. The uncertainty of the mass flow rate measurement was estimated to be roughly 3% following the propagation of uncertainty principle taking into account the uncertainty of the volume $V_{A,B}$, the temperature T_0 and pressure $P_{A,B}$ measurements. A more detailed description of the uncertainty estimation is outlined in [11]. The experiments were carried out in a temperature-controlled room ($T = 293.15\mathrm{K} \pm 0.5\mathrm{K}$), justifying the assumption of isothermal conditions in the volumes $V_{A,B}$. Details on the method can be found in [11, 12].

3 Numerical Modeling

The simulated flow setup includes the TPP structure (i.e., the tapered tube) and the substrate area (Fig. 4). The modeling domain corresponds to the physical domain extracted from tomography measurements. In the present model, the open borders (dashed lines) of the channel were maintained at different pressures (P_A and P_B). Two flow directions were considered: the converging flow with $P_A > P_B$ and the diverging flow with $P_A < P_B$, with the corresponding pressure ratio π defined as P_B/P_A and P_A/P_B respectively. In the modeling, the temperature of the solid walls and the gas at the open boundaries were maintained constant at $T_0 = 293.15$ K. Additionally, due to the axisymmetric nature of the flow, only a radial slice of the domain ($r > 0$) was considered. Thus, only two physical dimensions were taken into account, namely the $x-$ and $r-$ axis.

Based on the pressure values shown in Table 1b, the Knudsen number, calculated using the throat radius and the average pressure, ranges from 0.3 to 3.6. This suggests that the gas flow is in the transitional flow regime. In the present work, the Direct Simulation Monte Carlo method proposed by G. A. Bird [13] was applied to describe the flow behavior in the examined microstructure. Over the last few decades, it has evolved into a powerful and well-established numerical tool for studying phenomena over the whole range of the Knudsen number, making it well-suited for the flow problem addressed in this paper. For further details on the DSMC method the reader is referred to G. A. Bird's book [13]. In the present work, the effective collision scheme known as the No-Time-Counter (NTC) method, enhanced by the Variable Hard Sphere (VHS) model introduced by Bird, was used. The VHS model combines the simplicity of a hard-sphere scattering law with the flexibility of a variable collision cross-section, allowing for accurate representation of gas behavior under varying flow conditions. Based on the viscosity data for N_2 [14], the reference VHS diameter d_{ref} and the viscosity index ω for the examined flow conditions are taken as 4.11×10^{-10} m and 0.74 respectively. The gas-surface interaction was modeled based on the Diffuse-Specular model, in which a non-complete accommodation is assumed, while axisymmetric flow was also considered. By analyzing the available data in the literature on the accommodation coefficient α, it can be deduced that for typical technical surfaces without special treatment, a value between 0.9 and 1 is generally

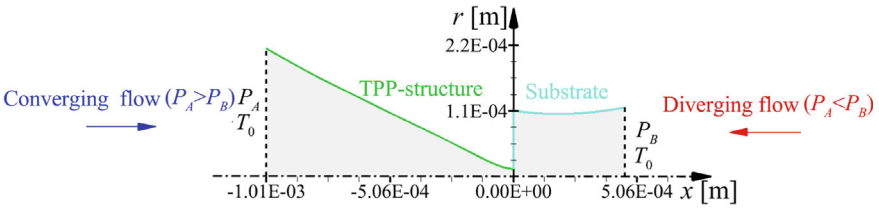

Fig. 4 Schematic view of the flow set-up considered in the present study. The gray area represents the computational domain

expected for N_2 [15, 16]. The computational grid consisted of 128,000 elements. The global cell size was $\Delta x = \Delta r = 1.34 \times 10^{-6}$ m, while in the region R = ($0 < r < 4 \times 10^{-5}$ m, -1.13×10^{-4} m $< x < 7.8 \times 10^{-5}$ m) the cell size was reduced three and six times in the $x-$ and $r-$ directions, respectively. It is noted that, cell size was chosen to be significantly smaller than the mean free path of the gas molecules. The number of DSMC particles varies from 33×10^6 to 40×10^6, with a minimum of at least 30 particles per cell. In order to maintain, as much as possible, uniform distributions of particles at each cell in the whole computational domain, the concept of the weighting factor widely applied in literature has been introduced. The time step Δt has been chosen to be sufficiently smaller (about 1/3) than the cell transversal time, defined as $\min(\Delta r, \Delta x)/u_0$ with u_0 being the most probable speed at reference temperature T_0 and Δr (or Δx) is the cell size in $r-$ (or $x-$) direction. The gas macroscopic quantities are obtained by time averaging over 10^7 time steps after the steady-state has been reached. In this type of pressure driven flows it is often essential to include two large reservoirs at the inlet and outlet of the channel to ensure the proper application of boundary conditions [5, 6, 8, 15]. For this specific setup, simulations using reservoirs up to eight times larger than the corresponding radius at the channel ends demonstrated no significant impact on the mass flow rate (within 1.5%). Consequently, the reservoirs are excluded from the configuration to save computational resources. The applied DSMC code has been successfully compared with results from kinetic models in [17].

4 Results and Discussion

In Fig. 5, a comparison between the DSMC data and the corresponding experimental ones is performed for both converging and diverging flow set-ups. The numerical and experimental data are in very good qualitative agreement for both configurations. As for the reference case, namely, $\alpha = 1$ and reference radius function $R(x)$ (see Table 1a), the comparison shows a consistent error of approximately 20%, which, while not negligible, is within an acceptable range given the geometrical fabrication complexity and the challenges associated with its experimental characterization. It is noted that, the DSMC results consistently underestimate the experimental results. To investigate and understand the sources of this deviation, we first examine the assumption of diffuse boundary conditions. For this purpose, we performed additional simulations assuming incomplete accommodation on the wall, with an accommodation coefficient $\alpha = 0.9$, which stands as the lowest expected value for the considered flow conditions. The corresponding results for $\alpha = 0.9$ are also shown in Fig. 5 for comparison purposes. As it is seen, a decrease in the accommodation coefficient of about 10% causes an increase in the mass flow rate about 10% bringing the DSMC data closer to the experimental ones. This can be considered the maximum uncertainty associated with the imposed pure diffuse boundary conditions.

Another important aspect that we investigated is the potential uncertainty related to the precise definition of the geometry, which remains challenging due to the small

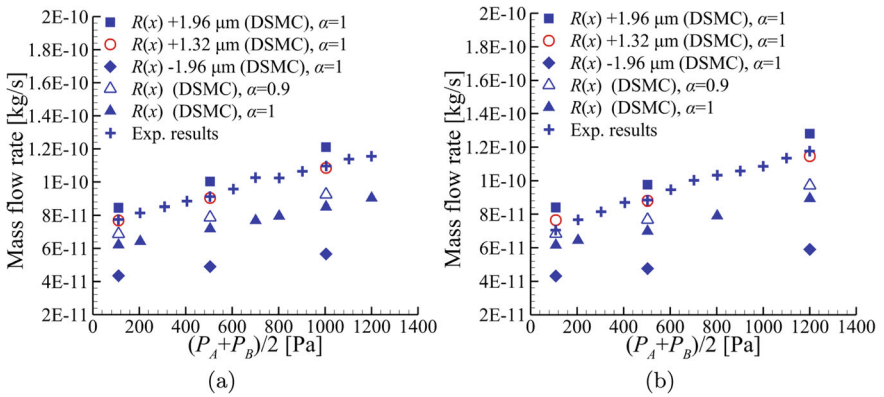

Fig. 5 Comparison of the mass flow rate between the DSMC and the experimental results for converging **a** and diverging **b** flow

scale of the channel. The uncertainty related to this measurement was estimated via a propagation of uncertainty principle. The radius measurement can be understood as a distance between two points. The position of either point has an uncertainty of $\pm dx/2$ (i.e. dx is the voxel size). Assuming both position measurements are not correlated, the uncertainty on the distance measurement is 1.96 μm corresponding to $\pm\sqrt{2}dx/2$. Additional simulations were performed by adding and subtracting 1.96 μm to the radius at each point in the flow direction, corresponding to the estimated uncertainty of the geometry measurement. As it is observed, the geometry uncertainties affect significantly the comparison between DSMC and experimental results. However, the experimental data are always within the two limits imposed by the DSMC simulations, with the experimental results showing better agreement with the larger radius geometry. Based on the above findings we can conclude that an acceptable agreement between the DSMC and experimental data is achieved, given the uncertainties associated with the geometry characterization and gas surface interaction modeling. Based on the mass flow rate data shown in Fig. 5, an attempt was made to estimate the potential radius increase required to obtain acceptable agreement between DSMC and experiments. Interpolation of the data showed that a uniform increase of 1.32 μm resulted in a very good agreement between the experimental and DSMC results with an average error over the entire pressure range of about 2%. This holds true for both examined flow configurations in a very consistent manner. For the sake of clarity and consistency, the corresponding results with $R(x)$+1.32 μm are also shown in Fig. 5. This level of agreement highlights the capability of such a kinetic modeling to complement experimental investigations, particularly in scenarios where the precise definition of the geometry is challenging due to the small scale of the channel.

Figure 6 shows indicative pressure and velocity contours for both converging and diverging flows for the case 1 of Table 1b. This case corresponds to the one with the largest inlet-to-outlet pressure ratio, namely $\pi \approx 0.05$. The velocity contours

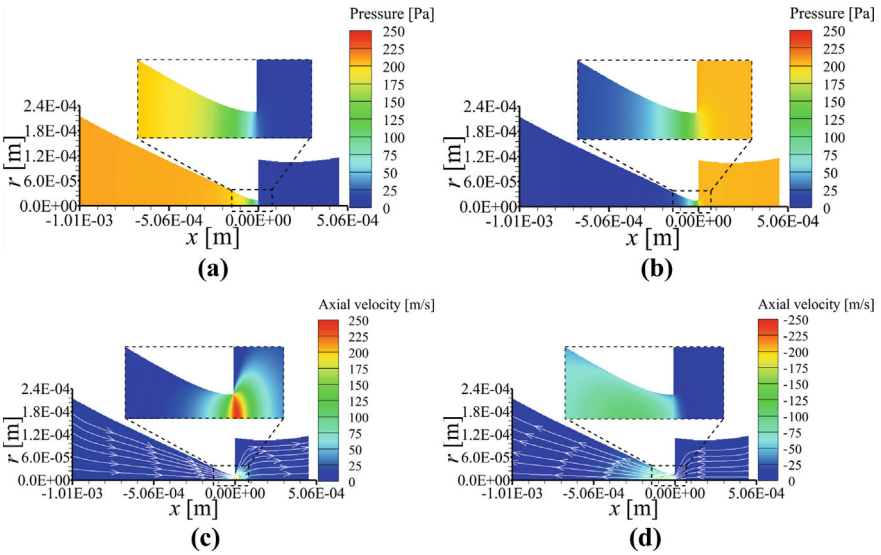

Fig. 6 Contours of pressure **a**, **b** and velocity **c**, **d** for converging **a**, **c** and diverging **b**, **d** flow, for case 1 ($\pi = 0.05$)

are overlaid by the velocity streamlines. The results show that for both pressure and axial velocity, the greatest variations are observed around the throat at $x = 0$. Similar qualitative behavior was observed for all the examined cases in Table 1b. It is observed that the radial pressure change is not very significant, whereas the radial velocity change is more pronounced, with the maximum values always occurring close to the axis of symmetry $r = 0$, a well-known behavior due to the wall friction effects.

In order to gain a better quantitative understanding of the changes in the macroscopic quantities, the axial distributions of velocity, temperature and pressure are shown in Fig. 7. Two cases are plotted, namely case 1 with $\pi \approx 0.05$ and 8 with $\pi \approx 0.8$, which correspond to high and low inlet-to-outlet pressure ratios, respectively. As can be seen, the velocity remains uniform and noticeably small far from the throat, while it shows strong variations in the throat region. By comparing the velocity profiles of cases 1 and 8, it can be easily deduced that the velocity is an increasing function of the pressure difference. The local Mach number always remains below 0.7 in converging flow direction and below 0.3 in diverging flow direction. In the converging direction, as the gas moves toward the throat, the decreasing area causes it to accelerate (due to the conservation of mass). In the diverging flow, however, the opposite occurs: the gas velocity reaches its maximum after the throat due to expansion effects, and then decreases due to the less resistance to the gas flow as a consequence of the increase in the area. As stated above, the gas flow accelerates as it passes through the narrow area at throat, which leads to an increase in kinetic energy, and part of this energy is extracted from the thermal energy, resulting in

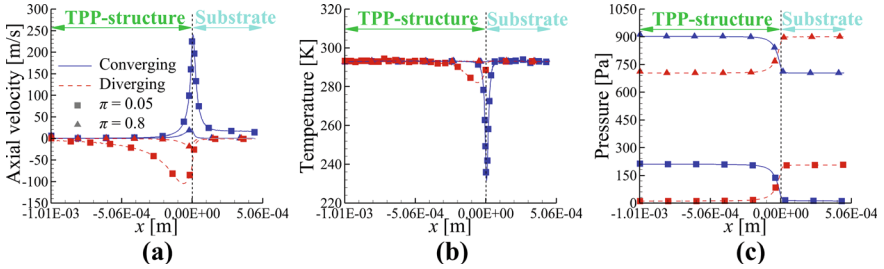

Fig. 7 Axial distributions of the axial velocity **a**, temperature **b** and pressure **c** at $r = 0$

a drop in temperature, as observed from the axial temperature distributions. It is noted that, as the inlet-to-outlet pressure drop decreases, the temperature of the gas flow approaches the wall temperature, and the flow shows isothermal characteristics. Finally, the axial pressure distributions show that the pressure remains uniform and close to its equilibrium values at the two entrances of the flow configuration, while a rapid change in pressure is observed near the throat, coinciding with the aforementioned increase in velocity.

5 Conclusions

This study presents, for the first time, a comparative analysis of experimental and numerical results for pressure-driven flows through micro-tapered tubes manufactured via two-photon-polymerization. The characterization of the flow is performed experimentally via the constant volume technique, as well as numerically via the DSMC method. A good comparison between the experimental and numerical data is observed, given all the uncertainties regarding the geometry characterization and the modeling assumptions which have been quantified in a detailed manner. This study shows that DSMC is a powerful tool for modeling rarefied gas flows in complex microstructures and for characterizing micro-device geometries in meso-scale configurations, where optical or X-ray measurements are challenging. In the future, we plan to extend both the experimental and numerical aspects of this analysis to more complex microstructures with varying cross-sections, relevant to aerospace and vacuum technologies.

Acknowledgements This work was carried out with the support of the Karlsruhe Nano Micro Facility (KNMFi, www.knmf.kit.edu), a Helmholtz Research Infrastructure at Karlsruhe Institute of Technology (KIT). The Research Federation FERMaT (FR 3089, Toulouse - France) is acknowledged for access to its Easy Tom XL X-ray tomograph. This work was supported by computational time granted from the National Infrastructures for Research and Technology S.A. (GRNET S.A.) in the National HPC facility - ARIS - under project ID pr015027-FUSFLOWSIM.

References

1. Alexeenko AA, Levin DA, Gimelshein SF, Collins RJ, Markelov GN (2002) Numerical simulation of high-temperature gas flows in a millimeter-scale thruster. J Thermophys Heat Transf 16. https://doi.org/10.2514/2.6667
2. López Quesada G, Tatsios G, Valougeorgis D, Rojas-Cárdenas M, Baldas L, Barrot C, Colin S (2020) Thermally driven pumps and diodes in multistage assemblies consisting of microchannels with converging, diverging and uniform rectangular cross sections. Microfluid Nanofluid 24:54 . https://doi.org/10.1007/s10404-020-02357-z
3. Sharipov F, Bertoldo G (2005) Rarefied gas flow through a long tube of variable radius. J Vac Sci Technol A 23:531–533. https://doi.org/10.1116/1.1897703
4. Graur I, Ho MT (2014) Rarefied gas flow through a long rectangular channel of variable cross section. Vacuum 101:328–332. https://doi.org/10.1016/j.vacuum.2013.07.047
5. Titarev VA, Shakhov EM, Utyuzhnikov SV (2014) Rarefied gas flow through a diverging conical pipe into vacuum. Vacuum 101:10–17. https://doi.org/10.1016/j.vacuum.2013.07.030
6. Tantos C, Litovoli F, Teichmann T, Sarris I, Day C (2024) Numerical study of rarefied gas flow in diverging channels of finite length at various pressure ratios. Fluids 9:78. https://doi.org/10.3390/fluids9030078
7. Ebrahimi A, Roohi E (2017) DSMC investigation of rarefied gas flow through diverging micro/nanochannels. Microfluid Nanofluid 21:18. https://doi.org/10.1007/s10404-017-1855-1
8. Sazhin O, Sazhin A (2023) Rarefied gas flow into vacuum through linearly diverging and converging channels. Int J Heat Mass Transf 203:123842. https://doi.org/10.1016/j.ijheatmasstransfer.2022.123842
9. Zhang D, López Quesada G, Bergdolt S, Hengsbach S, Bade K, Colin S, Rojas-Cárdenas M (2023) 3D micro-structures for rarefied gas flow applications manufactured via two-photon-polymerization. Vacuum 211:11915. https://doi.org/10.1016/j.vacuum.2023.111915
10. Graur I, Veltzke T, Méolans JG, Ho MT, Thöming J (2015) The gas flow diode effect: theoretical and experimental analysis of moderately rarefied gas flows through a microchannel with varying cross section. Microfluid Nanofluid 18:391–402. https://doi.org/10.1007/s10404-014-1445-4
11. Silva E, Deschamps CJ, Rojas-Cárdenas M, Barrot-Lattes C, Baldas L, Colin S (2018) A time-dependent method for the measurement of mass flow rate of gases in microchannels. Int J Heat Mass Transfer 120:422–434. https://doi.org/10.1016/j.ijheatmasstransfer.2017.11.147
12. Rojas-Cárdenas M, Silva E, Ho MT, Deschamps CJ, Graur I (2017) Time-dependent methodology for non-stationary mass flow rate measurements in a long micro-tube. Microfluid Nanofluid 21:86. https://doi.org/10.1007/s10404-017-1920-9
13. Bird GA (1994) Molecular gas dynamics and the direct simulation of gas flows. Clarendon Press, Oxford, Oxford Engineering Science Series
14. Boushehri A, Bzowski J, Kestin J, Mason EA (1987) Equilibrium and transport properties of eleven polyatomic gases at low density. J Phys Chem Ref Data 16:445-466. https://doi.org/10.1063/1.555800
15. Sharipov F (2016) Rarefied gas dynamics. Wiley-VCH Verlag GmbH & Co, KGaA, Weinheim, Germany
16. Yousefi-Nasab S, Safdari J, Karimi-Sabet J, Norouzi A, Amini E (2019) Determination of momentum accommodation coefficients and velocity distribution function for Noble gas-polymeric surface interactions using molecular dynamics simulation. Appl. Surf. Sci. 493:766–778. https://doi.org/10.1016/j.apsusc.2019.07.033
17. Tantos C, Varoutis S, Day C (2020) Deterministic and stochastic modeling of rarefied gas flows in fusion particle exhaust systems. J Vac Sci Technol B 38:064201. https://doi.org/10.1116/6.0000491